Polymer Chemistry

Accepted Manuscript

This article can be cited before page numbers have been issued, to do this please use: K. Raheja, S. Beilharz, A. Lalam, M. B. Hasan, D. Mathur and M. Karayilan, *Polym. Chem.*, 2026, DOI: 10.1039/D6PY00425C.

ROYAL SOCIETY OF CHEMISTRY

rsc.li/polymers

View Article Online
DOI: 10.1039/D6PY00425C

Thermoresponsive Fluorescent Polymers: Influence of Size, Composition, and Architecture

Konpal Raheja,[a] Sophia Beilharz,[a] Ajitesh Lalam,[a] Md. Bablu Hasan,[a] Divita Mathur,[a] Metin Karayilan[a, *]

[a] Department of Chemistry, Case Western Reserve University. Cleveland, OH 44106 USA

Abstract. Thermoresponsive fluorescent polymers (TFPs) provide a versatile platform for optical temperature sensing by coupling phase transitions with changes in fluorescence. Here, we report TFPs based on poly(*N*-isopropylacrylamide) (PNIPAM) and poly(ethylene glycol methacrylate) (PEGMA), incorporating fluorescein acrylate (FluA) as a model fluorophore via reversible addition-fragmentation chain transfer (RAFT) copolymerization. Linear and hyperbranched architectures were synthesized, with different compositions to position cloud point temperatures (T_{cp}) within a physiologically relevant temperature window, and their fluorescence behavior was investigated as a function of temperature, concentration, and pH. Distinct responses were observed across the T_{cp}, governed by the interplay between polymer collapse, microenvironmental confinement, and chromophore-chromophore interactions. Systems with low fluorescein loading exhibited fluorescence enhancement near the T_{cp} followed by quenching at higher temperatures, whereas higher loading systems showed predominantly decreased fluorescence intensity upon heating. Because all samples were compared at equal mass concentration, raw emission intensity scaled primarily with fluorophore loading per chain; we therefore interpret intensity differences cautiously and emphasize the temperature-dependent response as the diagnostic readout. Fluorescence intensity was strongly concentration-dependent, and pH studies revealed changes in both fluorescence intensity and emission maxima, with temperature-responsive fluorescence most prominent at pH 7 and moderately retained at pH 9. Rheological measurements further demonstrated changes in complex viscosity across the T_{cp}, linking macroscopic behavior to structural transitions. Hyperbranched polymers displayed responses distinct from their linear analogues. We summarize these observations as a set of provisional design rules that link each structural variable, such as composition, fluorophore loading, and architecture, to its dominant effect on T_{cp}, fluorescence, and viscosity. We note that several of these variables co-vary across the present sample set. Trends are therefore interpreted within controlled compositional windows rather than as fully orthogonal factors, and the resulting rules are intended as practical guidelines for designing polymer-based optical thermometers.

1. Introduction

Biological systems continuously operate under dynamic physicochemical conditions, where variations in temperature, pH, and the local microenvironment influence conformation, transport, and function. Accordingly, synthetic materials that respond to such biological cues in a controlled and reversible manner have emerged as powerful tools for interfacing with biological processes at the molecular level.[1-3] Among these adaptive materials, stimuli-responsive polymers have attracted sustained interest due to their ability

View Article Online
DOI: 10.1039/D6PY00425C

to undergo well-defined physicochemical transitions in response to external triggers, enabling applications ranging from controlled drug delivery to biosensing and intracellular imaging.[4-8] Although polymer responsiveness can be tailored to a range of stimuli, temperature remains one of the most widely used triggers in biomedical applications because it leverages the difference between room and physiological temperatures.[9] Temperature-responsive (thermoresponsive) polymers that undergo a reversible phase transition in aqueous solution upon increasing temperature have played a crucial role in advancing many biomedical and materials science applications.[10-16] Polymers with lower critical solution temperature (LCST) behavior undergo a coil-to-globule transition, shifting from soluble to insoluble as the temperature crosses the LCST. Heating disrupts polymer-water hydrogen bonding, altering the hydrophilic-hydrophobic balance and driving this phase transition. Polymers with an LCST near physiological temperature are of great interest, enabling injectable biomaterials that form viscous fluids or soft gels upon injection into the human body.[17]

Since the seminal report on the thermoresponsive properties of poly(*N*-isopropylacrylamide) (PNIPAM),[18] it has been extensively studied due to its distinctive temperature-dependent phase-transition behavior.[10, 19-22] PNIPAM exhibits an LCST of approximately 32 °C in water, making it ideal for biomedical applications as it remain soluble at room temperature but phase-separates at body temperature (37 °C),[19, 23, 24] and PNIPAM-based biomaterials have been widely explored for drug delivery, tissue engineering, and wound healing.[11-17] More recently, poly(ethylene glycol) methacrylate (PEGMA) copolymers have emerged as promising alternatives owing to their potential biocompatibility and tunable LCST.[25-27] A key advantage of PEGMAs is that the LCST of copolymers can be tuned by modifying the length of the ethylene glycol side chain.[28] These copolymers show reversible phase transitions with minimal hysteresis and are relatively insensitive to concentration, ionic strength, and chain length, positioning them as a complementary class of thermoresponsive polymers to PNIPAM.[29]

Building on these thermoresponsive platforms, considerable effort has been directed toward coupling the phase-transition behavior with optical readouts to enable real-time monitoring of the polymer's environment. Among the available signal-transduction strategies, fluorescence-based systems offer high sensitivity, ease of detection, and the ability to monitor environmental changes such as temperature and chemical conditions.[30] Fluorescent polymers, formed by incorporating fluorophores into polymer chains, further enhance these capabilities through high photostability, strong emission, and resistance to photobleaching.[31, 32] Fluorescein, a commonly used fluorophore, absorbs blue light near 494 nm and emits green light near 512 nm, is visible to the human eye, and shows good biocompatibility at low concentrations.[33] As a small-molecule dye, however, its response is limited to reporting the environment without intrinsic responsiveness.

View Article Online
DOI: 10.1039/D6PY00425C

Thermoresponsive fluorescent polymers (TFPs), by contrast, integrate fluorophores within a polymer matrix, enabling coupled optical and thermoresponsive behavior. These systems have emerged as promising multifunctional materials with applications in fluorescent temperature sensing, cellular imaging, drug delivery, and biometric identification.[34-38] Fluorescence-based thermometry provides a non-contact route to temperature measurement with high spatial and temporal resolution, including in environments where conventional probes are impractical.[39-44] Dual-responsive fluorescent probes that respond to both temperature and pH further expand the utility in complex biological environments where multiple stimuli coexist.[45-48]

Temperature influences fluorescence primarily through changes in polymer conformation and aggregation.[49] Conformational variation can alter emission wavelength,[49-52] while temperature-dependent aggregation strongly modulates intensity.[34, 35, 53-57] At higher concentrations or under conditions that promote intermolecular interactions, aggregation-caused quenching (ACQ) may occur due to π-π stacking and enhanced non-radiative decay pathways,[54-56, 58] whereas systems exhibiting aggregation-induced emission (AIE) show increased fluorescence upon aggregation as restricted intramolecular motion suppresses non-radiative energy dissipation.[59, 60] These competing effects highlight the importance of controlling polymer architecture and intermolecular interactions to achieve desirable thermoresponsive fluorescence behavior.

In this context, polymer topology is a key structural parameter for tuning such responses. Building on this idea, hyperbranched polymers offer a structurally distinct alternative to linear architectures through their highly three-dimensional, densely packed frameworks.[61-65] Unlike linear polymers, hyperbranched architectures inherently provide confined microenvironments and reduced chain mobility,[66, 67] which can significantly influence polymer conformation, chromophore interactions, and local polarity during thermally induced phase transitions.[68] This structural confinement can suppress non-radiative decay pathways while simultaneously promoting inter- or intramolecular interactions, thereby enabling a tunable fluorescence response.[53, 54, 69] Notably, these architectural features also give rise to distinct rheological behavior, as the compact, low-entanglement structure of hyperbranched polymers governs their viscosity and flow response.[61, 70-72] As a result, hyperbranched thermoresponsive polymers present an opportunity to introduce topology-driven control over both fluorescence behavior and macroscopic properties.

Despite growing interest in TFPs, systematic studies that decouple the effects of polymer backbone chemistry, fluorophore loading, and macromolecular architecture remain limited. Direct comparisons between PNIPAM- and PEGMA-based systems, despite their distinct hydration and phase transition behavior, are particularly scarce, especially regarding temperature-based fluorescence modulation and coupled

View Article Online
DOI: 10.1039/D6PY00425C

physicochemical properties. Moreover, the influence of hyperbranched architecture on temperature-dependent fluorescence, pH responsiveness, and rheological behavior remains insufficiently understood. In this work, we address these gaps by systematically investigating TFPs across two widely studied thermoresponsive polymer families (PNIPAM and PEGMA), while varying the fluorophore composition (by changing the fluorescein acrylate comonomer feed ratio) and macromolecular architecture (linear vs. hyperbranched) (**Figure 1**). Because synthetic constraints prevent every variable from being changed in strict isolation, we interpret trends within controlled compositional windows and, throughout, distill the observations into provisional design rules linking each structural variable to its dominant effect on T_{cp}, fluorescence, and viscosity. By correlating fluorescence response, aggregation behavior, and viscosity changes across temperature and pH, this study elucidates how polymer topology and composition collectively govern structure-property relationships in thermoresponsive polymer systems.

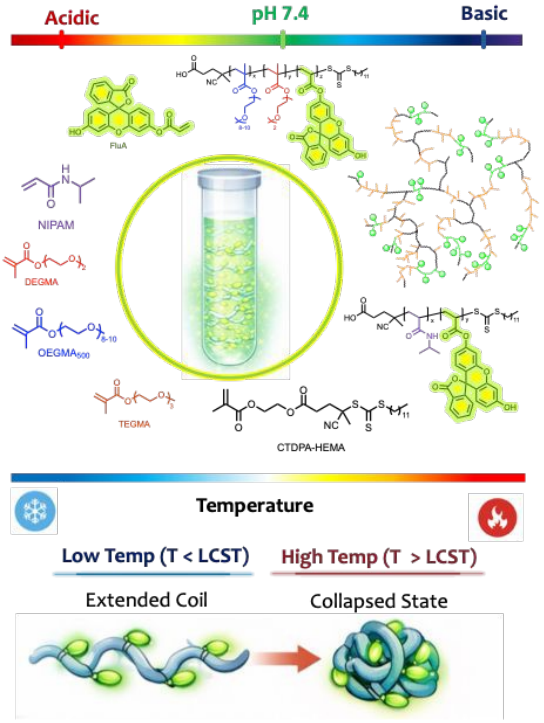

Figure 1. Schematic representation of the design and stimuli-responsive behavior of thermoresponsive fluorescent polymers (TFPs). The chemical structures of the monomers and corresponding linear and hyperbranched copolymers are shown, incorporating fluorescein acrylate as the fluorescent probe. The polymers are subjected to temperature and pH variation to record their fluorescence.

2. Results and Discussion

2.1. Synthesis of Thermoresponsive Fluorescent Polymers (TFPs)

To investigate how polymer functionality, composition, molecular weight, and architecture influence thermoresponsive fluorescence, a series of fluorescently labeled

View Article Online
DOI: 10.1039/D6PY00425C

polymers was synthesized. While complete orthogonal decoupling of these variables is experimentally challenging, trends are interpreted within controlled compositional windows and architectures. Building on the considerations outlined above, two thermoresponsive platforms were selected: PNIPAM-based systems, chosen for their well-defined LCST near physiological temperature, and PEGMA-based systems, which offer tunable thermal response through side-chain engineering. Fluorescein was used as a model fluorophore for its well-defined optical properties, exhibiting strong absorption in the blue region and green emission, resulting in copolymers that appear weakly yellow under ambient conditions but fluoresce bright green upon excitation. Within each platform, polymer molecular weight, comonomer composition, and architecture were varied to compare their effects on thermal and optical properties.

Initially, linear NIPAM-based TFPs[73-77] were synthesized to evaluate the effect of fluorescein incorporation on LCST behavior and temperature-dependent fluorescence. Linear P(NIPAM-*co*-FluA) copolymers containing low fluorescein loadings (1 and 5 mol% feed) were specifically designed to ensure sufficient fluorescence while minimizing disruption to PNIPAM's intrinsic hydrophilicity and thermal response (**Table 1**).[30, 78] Copolymers with 5 mol% (**$LP_{NIPAM}5$**) and 1 mol% (**$LP_{NIPAM}1$**) FluA were synthesized via reversible addition-fragmentation chain-transfer (RAFT) polymerization (**Figure 2A**).[79-81] Successful synthesis and purification of the copolymers were confirmed via proton (^{1}H) nuclear magnetic resonance (NMR) spectroscopy. The spectra showed the broad backbone resonances of PNIPAM together with fluorescein aromatic signals (7.0-8.0 ppm) and complete disappearance of vinyl monomer signals. Compositions were quantified from the PNIPAM methine proton (Hb, ~3.9 ppm) and the fluorescein aromatic proton (Ha, ~8.0 ppm) (**Figure 2A**); detailed assignments are given in the SI (Figures S1, S3).

View Article Online
DOI: 10.1039/D6PY00425C

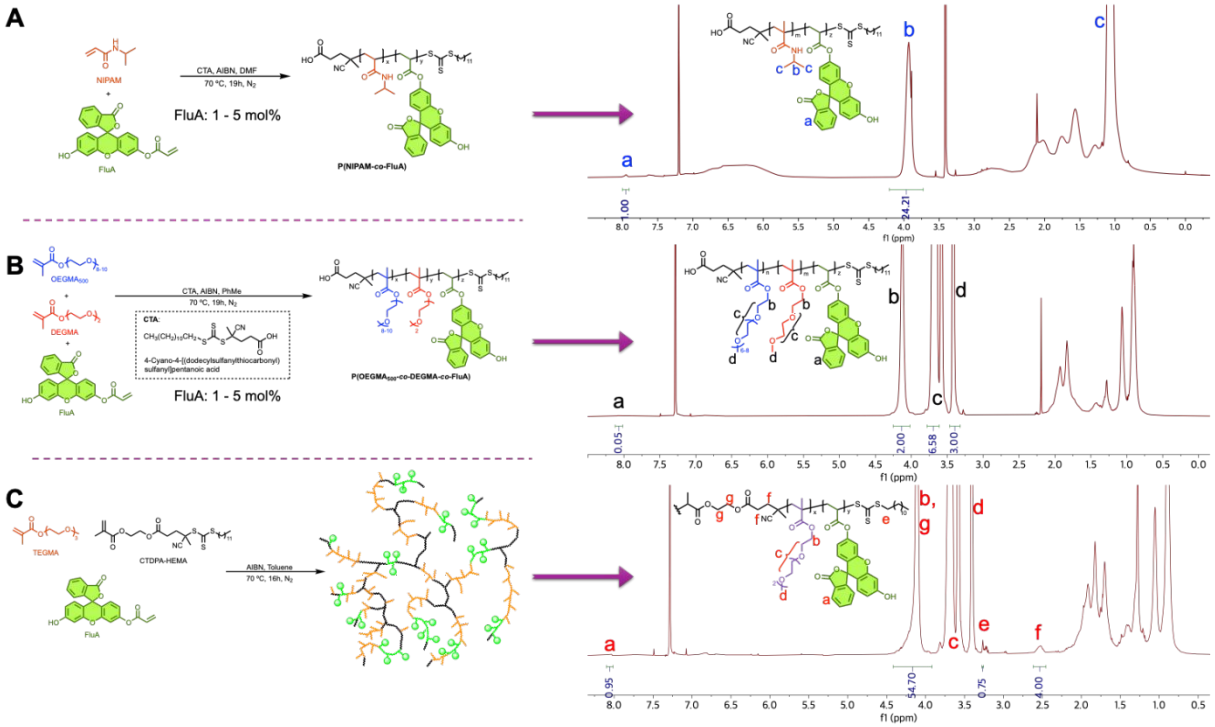

Figure 2. ^{1}H NMR spectra of FluA-containing thermoresponsive copolymers in $CDCl_3$ at room temperature. **(A)** Linear, $LP_{NIPAM}1$: P(NIPAM$_{99}$-*co*-FluA$_1$) (1 mol% FluA feed), **(B)** linear, $LP_{EGMA}5$: P(OEGMA$_{10}$-*co*-DEGMA$_{89}$-*co*-FluA$_1$), and **(C)** hyperbranched, $HBP_{EGMA}1$: P(TEGMA$_{94}$-*co*-CTDPA-HEMA$_5$-*co*-FluA$_1$)

To extend the platform beyond PNIPAM, ethylene glycol methacrylate-based copolymers were synthesized, tuning thermal response through comonomer composition using monomers such as oligo(ethylene glycol) methacrylate (OEGMA), diethylene glycol monomethyl ether methacrylate (DEGMA), and triethylene glycol methacrylate (TEGMA). Longer ethylene glycol side chains increase hydrophilicity and thus raise the LCST;[23, 82] for example, OEGMA/DEGMA copolymers span LCST values from ~26 °C (PDEGMA homopolymer) to ~90 °C (POEGMA) depending on composition.[29, 83] Holding DEGMA content between 80 and 90 mol% maintained aqueous solubility while positioning the cloud point temperature (T_{cp}, defined as the temperature at which transmittance falls to 90%)[84, 85] near the physiologically relevant range. Two linear terpolymers, P(OEGMA-*co*-DEGMA-*co*-FluA) (**$LP_{EGMA}5$**, 5:90:5) and P(OEGMA-*co*-DEGMA-*co*-FluA) (**$LP_{EGMA}1$**, 10:89:1) (**Table 1**) were synthesized to probe the influence of comonomer ratio and fluorophore loading on thermoresponse and temperature-dependent fluorescence behavior (**Figure 2B**). Small deviations between feed and measured composition reflect differing monomer reactivity ratios. Synthesis, purification, and composition were confirmed by ^{1}H NMR, with DEGMA/OEGMA contents resolved from the methoxy (H_d, ~3.4 ppm), ester-adjacent methylene (H_b, ~4.1 ppm), and ethylene glycol backbone (H_c, ~3.6 ppm) signals, and FluA quantified from its aromatic proton (~8.0 ppm); full assignments appear in the SI (Figures S15, S24).

View Article Online
DOI: 10.1039/D6PY00425C

In addition to the linear systems, two hyperbranched analogues were synthesized to probe the influence of topology on thermoresponsive and optical behavior: a NIPAM-based system ($HBP_{NIPAM}1$, P(NIPAM-*co*-CTDPA-HEMA-*co*-FluA), 94:5:1) and an ethylene glycol-based system ($HBP_{EGMA}1$, P(TEGMA-*co*-CTDPA-HEMA-*co*-FluA), 94:5:1) (**Figure 2C**) prepared by self-condensing vinyl RAFT polymerization[86-88] using a CTDPA-HEMA chain transfer monomer (CTM) conjugate. The CTM carries both a RAFT chain-transfer moiety and a polymerizable vinyl group, so that pendant vinyl groups on growing chains undergo further propagation, linking chains into a hyperbranched architecture through combined chain- and step-growth processes; branching density is set by the monomer-to-CTM feed ratio.[89-92]

For the ethylene glycol methacrylate-based hyperbranched system, TEGMA was used in place of the OEGMA/DEGMA combination of the linear terpolymers. The bulky OEGMA side chains could introduce steric hindrance during SCVP and potentially reduce successful branching, whereas DEGMA alone would provide insufficient aqueous solubility. Although TEGMA gives a relatively high T_{cp} (~45 °C) in linear architectures (Figure S55) and so was not used alone in the linear TFPs, branching and end-group effects are expected to lower its cloud point,[61] making it a practical intermediate monomer that maintains ethylene glycol character and thermoresponsive behavior near the physiological range. For $HBP_{EGMA}1$, ^{1}H NMR confirmed incorporation of the CTDPA-HEMA branching unit (H_f, ~2.5 ppm; H_e, ~3.25 ppm) alongside TEGMA, with relative incorporation and FluA content quantified as described above (**Figure 2C**).

While the $HBP_{EGMA}1$ was sufficiently water-soluble for thermoresponsive and fluorescence studies, the NIPAM-based hyperbranched polymer $HBP_{NIPAM}1$ showed limited solubility in aqueous media. This reduced solubility may arise from the high density of hydrophobic trithiocarbonate RAFT end groups with a long hydrocarbon chain (dodecyl) located near the polymer periphery, which can strongly influence aqueous behavior in hyperbranched RAFT-derived systems. Similar end-group effects have been reported to alter cloud points and solution behavior in hyperbranched thermoresponsive polymers.[91] End-group removal (SI, Section 4.2) modestly improved water compatibility, but $HBP_{NIPAM}1$ remains soluble only at low concentration (0.1 mg/mL), sufficient for fluorescence measurement but not for the higher concentrations required for cloud-point and temperature-dependent fluorescence studies. $HBP_{NIPAM}1$ was therefore excluded from the quantitative thermoresponsive comparisons below.

Table 1. Structural characteristics of synthesized PNIPAM- and poly(ethylene glycol methacrylate)-based thermoresponsive fluorescent polymers, including polymer architecture, composition, and size, highlighting the range of linear and hyperbranched PNIPAM- and PEGMA-based systems investigated in this study.

Acronym[a]	Architecture	Polymer	Target Ratio	Composition[b]	M_n[c]
PNIPAM copolymers					

View Article Online
DOI: 10.1039/D6PY00425C

$LP_{NIPAM}5$	Linear	P(NIPAM-*co*-FluA)	95:5	94.8:5.2	342.4 kDa
$LP_{NIPAM}1$	Linear		99:1	96.0:4.0	273.4 kDa
$HBP_{NIPAM}1$	HB[d]	P(NIPAM-*co*-CTDPA-HEMA-*co*-FluA)	94:5:1	90.6:5.7:3.7	10.7 kDa
PEGMA copolymers					
$LP_{EGMA}5$	Linear	P($OEGMA_{500}$-*co*-DEGMA-*co*-FluA)	5:90:5	6.5:82.3:11.2	113.0 kDa
$LP_{EGMA}1$	Linear	P($OEGMA_{500}$-*co*-DEGMA-*co*-FluA)	10:89:1	16.3:80.8:2.9	198.3 kDa
$HBP_{EGMA}1$	HB	P(TEGMA-*co*-CTDPA-HEMA-*co*-FluA)	94:5:1	92.9:3.6:3.5	40.0 kDa

[a] The polymers are denoted by their target ratio: $LP_{NIPAM}5$: P($NIPAM_{95}$-*co*-$FluA_5$), $LP_{NIPAM}1$: P($NIPAM_{99}$-*co*-$FluA_1$), $HBP_{NIPAM}1$: P($NIPAM_{94}$-*co*-CTDPA-$HEMA_5$-*co*-$FluA_1$), $LP_{EGMA}5$: ($OEGMA_5$-*co*-$DEGMA_{90}$-*co*-$FluA_5$), $LP_{EGMA}1$: ($OEGMA_{10}$-*co*-$DEGMA_{89}$-*co*-$FluA_1$), $HBP_{EGMA}1$: P($TEGMA_{94}$-*co*-CTDPA-$HEMA_5$-*co*-$FluA_1$), [b] composition via ^1H NMR spectroscopy, [c] M_n: number-average molecular weight via size exclusion chromatography, and [d] HB: hyperbranched.

2.2. Characterization of TFPs

Phosphate-buffered saline (PBS, pH 7.4) was used as the measurement medium for all studies to ensure physiological relevance and stable pH conditions throughout the experiments.[93] Because fluorescein exhibits pronounced pH-dependent optical properties, even minor pH fluctuations can significantly alter its emission intensity and spectral characteristics.[94-96] The use of PBS, therefore, minimizes pH drift and ensures that observed fluorescence changes arise from thermoresponsive polymer behavior rather than uncontrolled changes in fluorophore protonation. Measuring in PBS also reflects biologically relevant ionic strength: salt identity and concentration influence hydration, LCST, and aggregation dynamics,[97, 98] so evaluating T_{cp} and fluorescence modulation in buffered saline ensures the transitions reflect application-relevant conditions (**Table 2**).

Table 2. Thermoresponsive and fluorescence characteristics of the polymer systems, including cloud point temperature (T_{cp}), estimated fluorescein loading per chain, and effective fluorophore concentration ([FluA]) at 0.1 and 5 mg/mL.

Acronym	T_{cp} (°C)	FluA per chain	[FluA] (μM, 0.1 mg/mL)	[FluA] (mM, 5 mg/mL)	DLS onset temperature
$LP_{NIPAM}5$	30.3	~139	40.4	2.0	32.8
$LP_{NIPAM}1$	29.6	~87	35.6	1.6	30.4
$HBP_{NIPAM}1$	Insoluble	-	-	-	-
$LP_{EGMA}5$	26.7	~54	47.8	2.39	29.8
$LP_{EGMA}1$	34.3	~23	11.8	0.59	36.4
$HBP_{EGMA}1$	34.1	~6	14.2	0.71	35.8

Absorbance and Fluorescence Analysis. The optical properties were first evaluated by recording their absorbance and fluorescence spectra in PBS (0.1 mg/mL) at room temperature (**Figure 3A**). All samples exhibit the characteristic absorption bands corresponding to the incorporated fluorophore (i.e., fluorescein), confirming successful functionalization. The fluorescence emission spectra show well-defined maxima at

View Article Online
DOI: 10.1039/D6PY00425C

comparable wavelengths, indicating that the fluorophore retains its intrinsic photophysical properties upon incorporation into the polymer matrix. However, clear differences are observed in fluorescence intensity depending on polymer type and structural parameters. Clear differences in emission intensity and spectral shape were observed between the PNIPAM- and PEGMA-based polymers. Because all spectra were recorded at the same polymer mass concentration rather than at matched fluorophore concentration, the dominant determinant of raw emission intensity is expected to be the number of emissive fluorophores present, which differs substantially across samples (**Table 2**). We therefore treat absolute intensity comparisons cautiously and do not assign intensity differences to chain length or topology in isolation; instead, the more informative comparisons are spectral shape, emission maximum, and, most importantly, the temperature-dependent response described below, which is largely decoupled from static fluorophore count.[68] Consistent with this, the highest-loading samples (e.g., $LP_{NIPAM}5$) show the strongest raw emission, and no significant spectral shifts accompany changes in loading, indicating that loading primarily affects emission magnitude rather than fluorophore electronic structure. A residual, loading-independent enhancement for the more solvated PEGMA backbone and for the confined hyperbranched $HBP_{EGMA}1$ (which emits more strongly than its linear counterpart of comparable per-chain loading) is consistent with reduced self-interaction and restricted fluorophore mobility, respectively; we present these as qualitative trends rather than quantitative attributions. At equal mass concentration, room-temperature emission intensity is set primarily by fluorophore loading per chain; backbone solvation (PEGMA > PNIPAM) and hyperbranched confinement act as secondary, per-fluorophore modifiers. Intensity alone is therefore not a reliable structural fingerprint—the temperature response is.

View Article Online
DOI: 10.1039/D6PY00425C

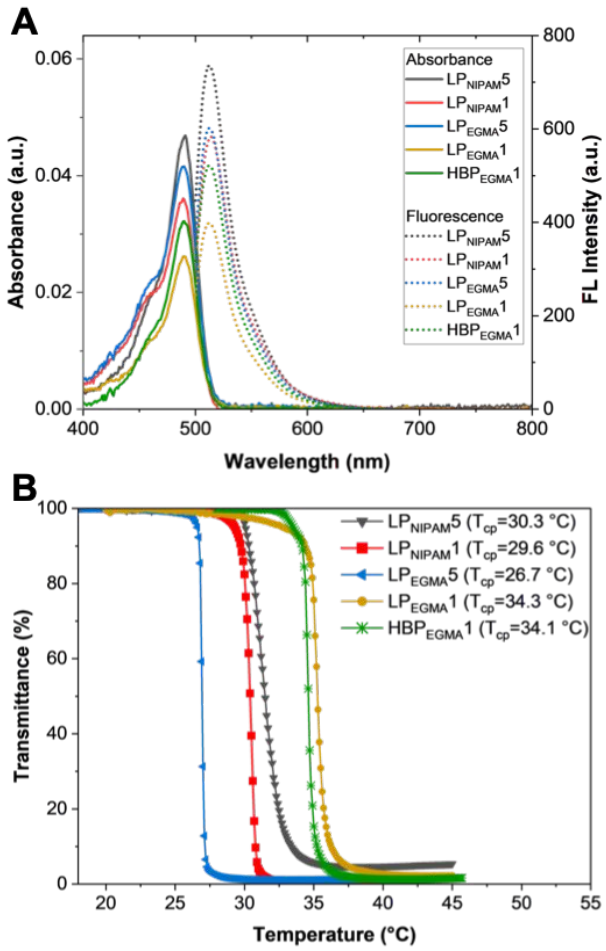

Figure 3. **(A)** Absorbance and fluorescence spectra of copolymers in PBS at 0.1 mg/mL at room temperature. **(B)** Cloud point temperature (T_{cp}) profiles in PBS at 1 wt% (10 mg/mL). LP_{NIPAM} samples correspond to linear PNIPAM copolymers: $LP_{NIPAM}5$ (linear, P(NIPAM-*co*-FluA), 95:5), and $LP_{NIPAM}1$ (linear, P(NIPAM-*co*-FluA), 99:1). PEGMA-based polymers include $LP_{EGMA}5$ and $LP_{EGMA}1$, which are linear P(OEGMA-*co*-DEGMA-*co*-FluA) copolymers, and HBP_{EGMA}, a hyperbranched P(TEGMA-*co*-CTDPA-HEMA-*co*-FluA) polymer. These polymers were synthesized to compare the properties of linear vs. hyperbranched architectures and of NIPAM-based vs. ethylene glycol methacrylate-based thermoresponsive systems containing the FluA unit.

Cloud point temperature (T_{cp}) measurements. To further elucidate how structural parameters influence thermoresponsive phase behavior, T_{cp} of the polymers was measured across the series (**Figure 3B**). T_{cp} is governed by the temperature-dependent balance between polymer–water hydrogen bonding and intramolecular hydrophobic interactions and is strongly set by the hydrophilic-to-hydrophobic ratio of the backbone. At low temperatures, hydrophilic functionalities, such as amide groups in PNIPAM and ethylene glycol side chains in PEGMA systems, maintain hydrogen bonding with water, stabilizing the polymers in a hydrated, soluble state (notably, the PNIPAM amide acts as both donor and acceptor, whereas ethylene glycol oxygens act primarily as acceptors). On heating, these bonds are disrupted and hydrophobic moieties (isopropyl, DEGMA segments, fluorescein) dominate, driving dehydration, coil-to-

View Article Online
DOI: 10.1039/D6PY00425C

globule collapse, ultimately leading to aggregation and macroscopic turbidity at T_{cp}. Although the fluorescein group is predominantly hydrophilic in aqueous buffer in its ionized form, its aromatic structure contributes localized hydrophobic interactions that become more pronounced at higher loadings.[99]

The T_{cp} of the TFPs varied systematically as a function of backbone composition, fluorophore loading, and macromolecular architecture. The lowest T_{cp} (~26.7 °C) was observed for $LP_{EGMA}5$, consistent with its high DEGMA content and elevated fluorescein incorporation, both of which raise the overall hydrophobic character of the polymer and promote earlier phase separation. The linear $LP_{NIPAM}1$ exhibited a higher T_{cp} (~29.6 °C), reflecting the intrinsic LCST behavior of PNIPAM in aqueous media. This suggests that the hydrophilic-hydrophobic balance dominates over chain-length effects in determining the phase behavior of these linear PNIPAM-based systems. The small difference in T_{cp} between the two PNIPAM samples can be rationalized by their differing fluorescein content: under PBS (pH 7.4) fluorescein is largely ionized, and its charged form enhances polymer–water interactions, modestly increasing hydrophilicity and T_{cp}.[95, 100] The hyperbranched $HBP_{EGMA}1$ displayed a further increase in T_{cp}, highlighting the influence of branching architecture, which enhances chain-end density and hydration, thereby stabilizing the hydrated state to higher temperatures. The highest T_{cp} was measured for $LP_{EGMA}1$, where the increased OEGMA content enhances hydrophilicity relative to the $LP_{EGMA}5$ system and delays phase separation. Collectively, these results demonstrate that T_{cp} is governed by a delicate interplay between backbone chemistry, comonomer ratio, fluorophore loading, and polymer topology, with hydrophilicity and architectural effects playing dominant roles in modulating thermoresponsive behavior. Increasing hydrophilic content (higher OEGMA, lower DEGMA), lowering fluorescein loading, and adopting a hyperbranched architecture each raise T_{cp}; increasing DEGMA and fluorophore loading lower it. T_{cp} is thus tunable through the net hydrophilic-hydrophobic balance, with topology providing an additional upward shift via chain-end hydration.

Dynamic Light Scattering (DLS) analysis. The phase transition temperature of the synthesized TFPs was independently investigated using temperature-controlled dynamic light scattering (DLS), as shown in **Figure 4**, at a polymer concentration of 0.1 mg/mL in PBS, to monitor temperature-dependent changes in hydrodynamic size. For all soluble systems, an initial increase in particle size was observed at characteristic temperatures near their T_{cp} values, marking the onset of polymer aggregation. The onset temperature on DLS was observed at 30.4 °C for $LP_{NIPAM}1$ and 32.8 °C for $LP_{NIPAM}5$, consistent with their thermoresponsive behavior (i.e., T_{cp}). Similarly, the PEGMA-based systems exhibited transitions at 29.8 °C for $LP_{EGMA}5$ and 36.4 °C for $LP_{EGMA}1$, while the hyperbranched $HBP_{EGMA}1$ displayed a transition at 35.8 °C, consistent with its T_{cp} and comparable to its linear analogue. Notably, these transition temperatures are slightly higher than the T_{cp} values obtained from turbidity measurements (performed at 10 mg/mL), as expected from the more dilute DLS conditions, where reduced intermolecular interactions delay detectable aggregation. Overall, the DLS results are in good agreement with the T_{cp} trends, confirming that

View Article Online
DOI: 10.1039/D6PY00425C

the observed phase transitions arise from temperature-induced dehydration and aggregation of the polymer chains.

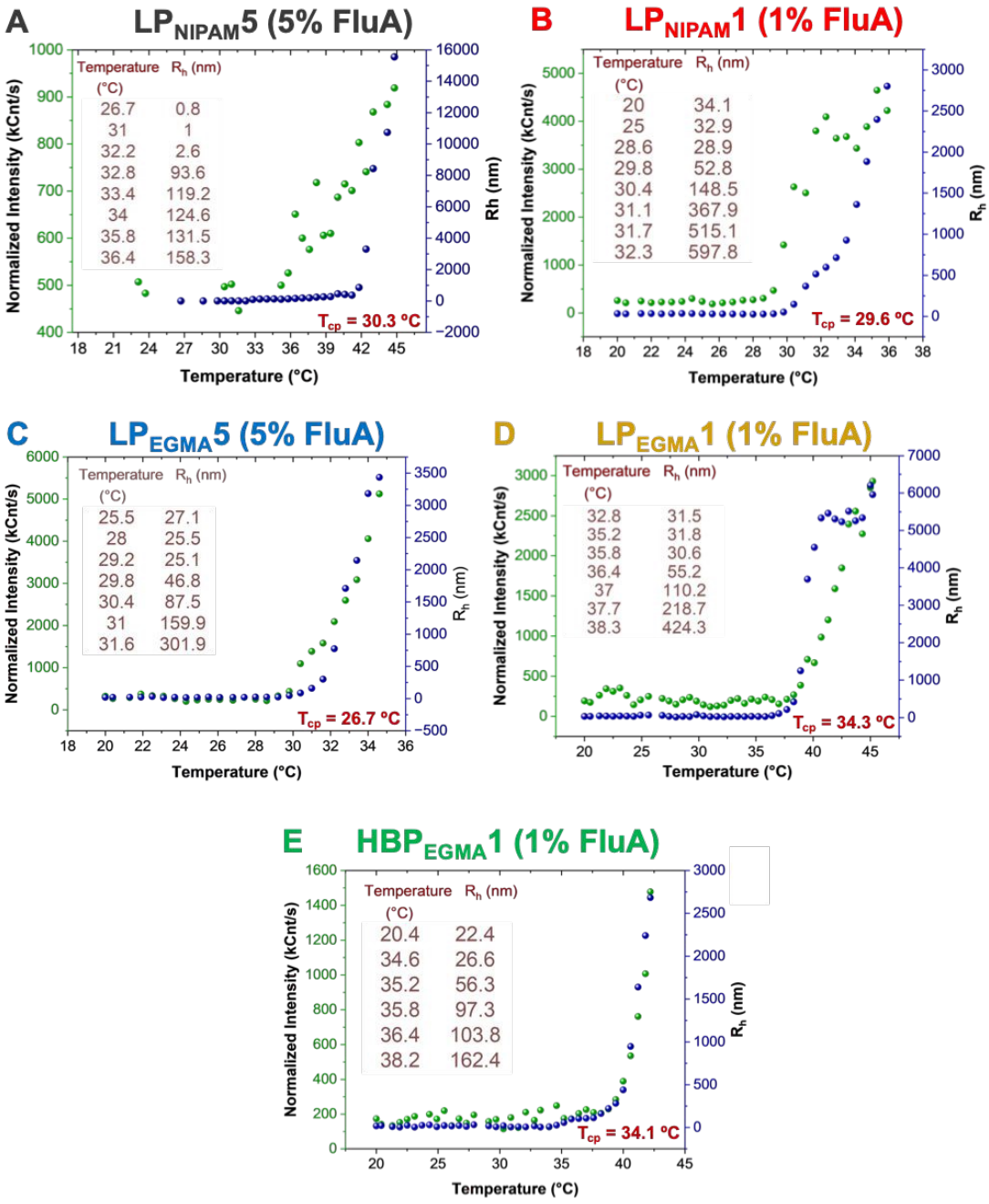

Figure 4. Hydrodynamic radius of TFPs **(A)** LP$_{NIPAM}$5 (5% FluA), **(B)** LP$_{NIPAM}$1 (1% FluA), **(C)** LP$_{EGMA}$5 (5% FluA), **(D)** LP$_{EGMA}$1 (1% FluA), and **(E)** HBP$_{EGMA}$1 (1% FluA) as a function of temperature obtained by dynamic light scattering (DLS) in PBS at 0.1 mg/mL.

Temperature-controlled UV-Vis absorption and fluorescence emission measurements. These analyses were performed to evaluate the thermal response of the copolymers in aqueous solutions. Upon heating, the absorbance profiles showed a gradual increase across the monitored wavelength

View Article Online
DOI: 10.1039/D6PY00425C

range. This behavior is consistent with the thermally induced phase transition of the polymers. Above T_{cp}, coil-to-globule collapse promotes aggregation and the formation of polymer-rich domains, leading to increased light scattering and an apparent elevation in baseline absorbance. Importantly, control experiments with free fluorescein in PBS (Figure S56) under identical temperature conditions showed no comparable increase in absorbance, confirming that the observed effect arises from thermoresponsive polymer aggregation rather than intrinsic temperature-dependent changes in the electronic absorption properties of the fluorophore.

To further validate this interpretation, additional control experiments were performed by physically mixing PNIPAM with a small amount of free fluorescein (Figure S57). In these mixtures, no significant change in fluorescence intensity was observed upon heating, despite a decrease in optical transmittance above the LCST due to polymer phase separation. This indicates that light scattering alone does not contribute to the observed fluorescence enhancement. Instead, the results confirm that covalent incorporation of fluorescein within the thermoresponsive polymer matrix is essential for coupling the LCST-driven structural transition to changes in fluorescence behavior.

Linear and hyperbranched thermoresponsive copolymers containing FluA were investigated at varying compositions. All fluorescence and absorbance measurements were conducted at a constant polymer concentration of 5 mg/mL in PBS using a 96-well plate reader; noting that the effective fluorophore distribution varied across systems (**Figure 5**). Importantly, all measurements were conducted in a microvolume format (50 µL in a 96-well plate), and the observed optical responses should be interpreted in this context, as larger path-length systems may exhibit different absorbance baselines and scattering contributions due to increased optical path length and sample volume.

The NIPAM-based polymers ($LP_{NIPAM}1$ and $LP_{NIPAM}5$) differ markedly in fluorophore content, with the $LP_{NIPAM}5$ sample containing ~139 fluorescein units per chain, compared to ~87 units for $LP_{NIPAM}1$, resulting in significant differences in intrachain crowding. Notably, such differences were not prominently reflected in the fluorescence behavior discussed above at lower polymer concentrations (0.1 mg/mL), likely due to the relatively dilute regime minimizing intermolecular interactions. In contrast, at higher concentrations (5 mg/mL), these effects became more pronounced, as increased local fluorophore density and polymer-polymer interactions amplify crowding and aggregation phenomena, thereby influencing the observed optical response. In contrast, the linear PEGMA copolymers ($LP_{EGMA}5$ and $LP_{EGMA}1$), composed of OEGMA and DEGMA with FluA, possess moderate molecular weights (~100-200 kDa) and intermediate fluorophore densities (~54 and ~23 fluorescein units per chain, respectively). The hyperbranched system (HBP_{EGMA}), based on TEGMA and a branching unit (CTA-monomer), differs both in architecture and composition, containing ~6 fluorescein units per chain and a low effective fluorophore concentration (~0.71 mM). Although this value is lower than that of linear PNIPAM systems and linear $LP_{EGMA}5$, it remains comparable to $LP_{EGMA}1$, allowing an informative

View Article Online
DOI: 10.1039/D6PY00425C

comparison while reflecting the reduced local fluorophore density within the hyperbranched architecture.

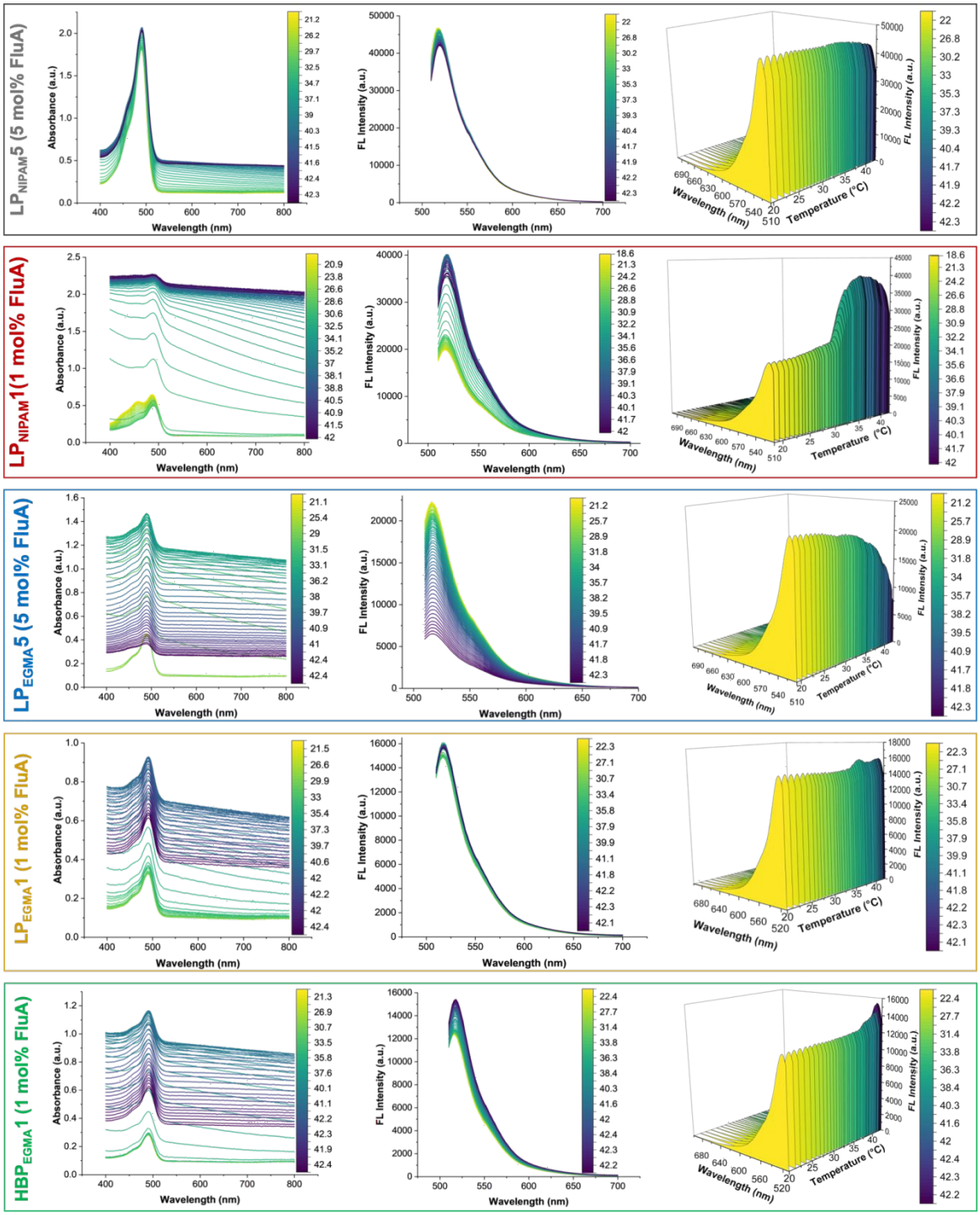

Figure 5. Absorption spectra (left), emission spectra (center), 3D representation of emission spectra (right) of TFPs in PBS obtained as a function of temperature from 18–42 °C at polymer concentration of 5 mg/mL using a 96-well plate.

View Article Online
DOI: 10.1039/D6PY00425C

Temperature-dependent fluorescence measurements revealed distinct structure–property relationships governed by polymer composition and architecture. The linear NIPAM systems displayed classical LCST behavior, with $LP_{NIPAM}1$ exhibiting a pronounced fluorescence increase near its cloud point (~30 °C) due to coil-to-globule transition and formation of hydrophobic microenvironments, whereas $LP_{NIPAM}5$ showed attenuated responsiveness due to strong intramolecular self-quenching arising from its high fluorophore density. The PEGMA-based copolymers ($LP_{EGMA}5$ and $LP_{EGMA}1$) exhibited more gradual fluorescence changes with temperature, reflecting differences in hydrophilicity and composition (OEGMA vs. DEGMA ratio), with $LP_{EGMA}5$ showing only a slightly higher fluorescence intensity despite its greater fluorophore content. This relatively modest increase may be attributed to the slightly higher molecular weight of $LP_{EGMA}1$, which can influence chain conformation and local microenvironment, partially offsetting the effect of increased fluorescein incorporation in $LP_{EGMA}5$. In contrast, the hyperbranched PEGMA system (HBP_{EGMA}), composed of TEGMA and branching units, displayed lower overall fluorescence intensity but a more gradual temperature response, consistent with reduced intrachain crowding and its distinct architecture (**Figure 6**). These results highlight that fluorescence response is dictated not only by the LCST transition (T_{cp} ~ 26.7-34.3 °C) but also by fluorophore distribution, composition, and architecture, with intramolecular crowding and local environment playing central roles. Importantly, all polymers displayed only a minor 2 nm red shift (516 →518 nm) on heating, also seen for free fluorescein in PBS and therefore attributed to general solvent-dependent thermal effects rather than aggregation-specific spectral reorganization. Overall, low fluorophore loading (~1 mol%) yields a strong fluorescence increase at the T_{cp} (collapse-driven confinement); high loading (~5 mol%) suppresses this response through chromophore self-quenching. Hyperbranching broadens and dampens the transition. Loading therefore selects the sign and sharpness of the thermoresponse, independent of which backbone family is used. To verify the reproducibility of these observations, multiple independent measurements were performed and analyzed statistically. The resulting error-bar plots (Figure S60) demonstrate good agreement between replicate experiments, confirming the reliability of the temperature-dependent fluorescence trends discussed above.

View Article Online
DOI: 10.1039/D6PY00425C

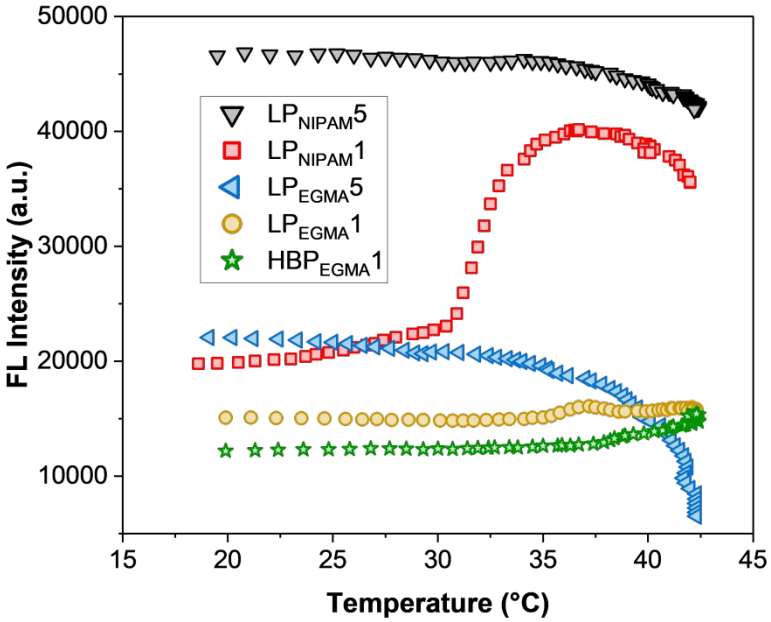

Figure 6. Temperature-dependent fluorescence intensity profiles of PNIPAM- and PEGMA-based TFPs obtained from the corresponding peak maxima (**Figure 5**) in the fluorescence emission (λ_{em} = 518 nm) spectra. Reproducibility analysis and associated error bars from replicate measurements are provided in Figure S60.

Concentration dependence. The thermoresponsive fluorescence behavior of selected low-fluorophore-content polymers, namely LP$_{NIPAM}$1, LP$_{EGMA}$1, and HBP$_{EGMA}$1, each containing approximately 1 mol% FluA, was evaluated as a function of concentration (1–20 mg/mL) (**Figure 7 A-C**). At low concentration (1 mg/mL), only minimal changes in fluorescence intensity were observed for all systems (Figures S12, S32, S51), indicating insufficient intermolecular interactions to induce significant thermoresponsive effects. For LP$_{NIPAM}$1, a pronounced increase in fluorescence intensity was observed near the T_{cp} at 5 mg mL, followed by a decrease at higher temperatures. This enhancement became progressively more pronounced at higher concentrations (10 and 20 mg/mL), indicating that increased polymer concentration promotes microenvironmental confinement and intermolecular interactions upon collapse. The subsequent decrease at higher temperatures suggests the onset of chromophore-chromophore interactions and non-radiative quenching.

View Article Online
DOI: 10.1039/D6PY00425C

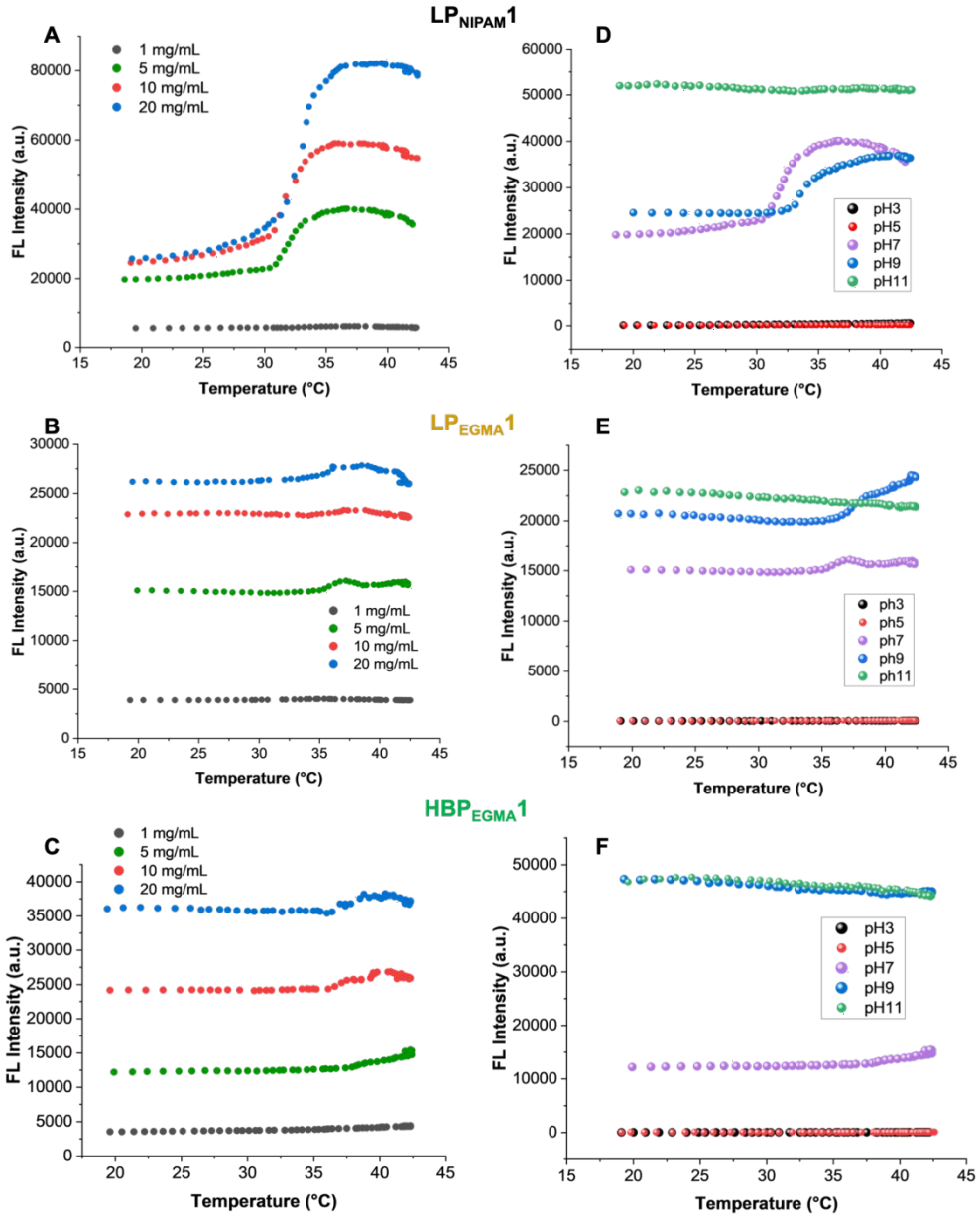

Figure 7. Temperature-dependent fluorescence intensity profiles of PNIPAM- and PEGMA-based systems containing 1 mol% FluA in PBS, evaluated as a function of concentration (1, 5, 10, and 20 mg/mL; panels A-C) and pH (3, 5, 7, 9, and 11; panels D-F). Fluorescence intensities were extracted from the emission maxima (λ_{em} = 518 nm for all samples, and 510 nm for pH 3 and 5) of the corresponding emission spectra.

A similar, but less pronounced, trend was observed for $LP_{EGMA}1$, with a modest increase in fluorescence intensity near the transition temperature at 5 mg/mL, followed by a decrease. At higher concentrations (10 and 20 mg/mL), the magnitude of fluorescence enhancement increased, consistent with increased aggregation and interaction-driven effects in the collapsed state. In contrast, the hyperbranched $HBP_{EGMA}1$ system exhibited delayed fluorescence enhancement at 5 mg/mL, with the increase occurring several degrees above the T_{cp}. At higher concentrations (10 and 20 mg/mL), a more pronounced increase followed by a decrease at elevated temperatures was

View Article Online
DOI: 10.1039/D6PY00425C

observed, suggesting that architectural confinement in the hyperbranched structure modulates the balance between fluorescence enhancement and quenching (**Figure 7C**). Aggregation is a prerequisite: pronounced thermoresponsive fluorescence emerges only above a threshold concentration (≳5 mg/mL). Linear chains respond at the T_{cp}; hyperbranched architecture shifts the onset to higher temperature, offering a topology-based handle on the response window.

pH dependence. The influence of pH on thermoresponsive fluorescence was investigated across pH 3-11 (**Figure 7D-F**). The T_{cp} of all PNIPAM and PEGMA polymers followed the trend: pH 5 < pH 3 < pH 7 < pH 9 < pH 11, indicating increased stabilization of the hydrated state at higher pH. The relatively lower T_{cp} values at pH 3 and pH 5 can be attributed to the use of acetate buffer systems, where acetate ions are known to promote polymer dehydration through salting-out effects,[22, 101] thereby facilitating earlier phase separation. The more pronounced decrease at pH 5 compared to pH 3 is consistent with the higher concentration of acetate anions at elevated pH within the buffer system. In contrast, at neutral and basic pH, the increased ionization of fluorescein enhances polymer-water interactions by introducing charged groups, leading to improved hydration and a corresponding increase in T_{cp}. These results highlight the combined influence of buffer composition and fluorophore ionization on thermoresponsive phase behavior.

At acidic conditions (pH 3 and 5), all polymers exhibited negligible fluorescence intensity despite a gradual increase with temperature. This behavior is attributed to reduced fluorescein emissivity under acidic conditions,[102] where the chromophore exists in less fluorescent protonated forms. Consistent with this, the wavelength of maximum emission was blue-shifted under acidic conditions (~510 nm) compared to neutral and basic pH (~518 nm), reflecting changes in the electronic state of fluorescein with pH. At a highly basic condition (pH 11), the fluorescence intensity was the highest among all pH values; however, no significant thermoresponsive change was observed. The temperature-dependent fluorescence profile closely resembled that of free fluorescein in solution, indicating that polymer collapse plays a minimal role under these conditions and that fluorescence is dominated by the intrinsic behavior of the fully deprotonated fluorescein species. At intermediate pH values (pH 7 and pH 9), clear thermoresponsive fluorescence behavior was observed. For $LP_{NIPAM}1$, a significant increase in fluorescence intensity was observed near the T_{cp}, with the onset occurring at higher temperatures for pH 9 compared to pH 7, consistent with the shift in cloud point with pH. A similar trend was observed for $LP_{EGMA}1$, where fluorescence enhancement followed the corresponding shift in phase transition temperature. In contrast, $HBP_{EGMA}1$ exhibited a distinct response, with fluorescence enhancement observed at pH 7, while at pH 9 only minimal changes were detected. This difference highlights the influence of polymer topology, where the hyperbranched architecture alters local microenvironmental sensitivity and modulates the balance between confinement-induced enhancement and interaction-driven quenching. Collectively, these results indicate that fluorescence modulation in these thermoresponsive systems is governed by a balance between microenvironmental dehydration (enhancement) and collapse-induced dye proximity (quenching), with fluorophore density and polymer architecture determining which mechanism predominates. Useful thermoresponsive

View Article Online
DOI: 10.1039/D6PY00425C

fluorescence requires the dye to be in its emissive, partly ionized state: it is maximal near neutral pH, retained at pH 9, and lost under acidic conditions (protonation) or strongly basic conditions (where the free-dye signal dominates and the polymer contribution vanishes).

Rheological Analysis. Rheological measurements were performed using a parallel plate rheometer to investigate the viscosity change of the linear and hyperbranched polymer systems as a function of angular frequency at room temperature (25 °C) and physiological temperature (37 °C) (**Figure 8**). In all cases, the complex viscosity decreased with increasing angular frequency, consistent with the expected shear-thinning behavior of associative polymer solutions. Importantly, both the PNIPAM- and PEGMA-based systems exhibited T_{cp} values near or below 37 °C and therefore displayed higher complex viscosity at 37 °C than at room temperature across the full frequency range. This increase in viscosity indicates that thermal activation does not simply reduce hydrodynamic volume but instead promotes interchain association and the formation of transient polymer-rich aggregates that enhance resistance to flow. Thus, above T_{cp}, increased interchains attractions induce polymer collapse, resulting in a more viscous solution state. Notably, polymers with higher cloud point temperatures, such as $LP_{NIPAM}5$ and $HBP_{EGMA}1$ (> 30 °C), exhibit a comparatively smaller increase in viscosity at 37 °C relative to systems with lower T_{cp} values (~26-29 °C), as they are closer to the onset of the phase transition and therefore experience less extensive collapse and interchain association under these conditions. In contrast, the hyperbranched PEGMA-based polymer exhibited a distinct deviation from the power-law frequency dependence observed for the linear analogues. While the linear polymers displayed typical shear-thinning behavior consistent with entangled chain dynamics, the hyperbranched system showed a more curved viscosity profile, reflecting its compact architecture, reduced entanglement, and altered viscoelastic relaxation behavior. Crossing the T_{cp} converts these solutions from less to more viscous (interchain association on collapse); the magnitude scales with how far above T_{cp} the measurement sits. Hyperbranching replaces entanglement-dominated shear-thinning with a compact, weakly-entangled flow signature—an architecture-specific rheological fingerprint.

View Article Online
DOI: 10.1039/D6PY00425C

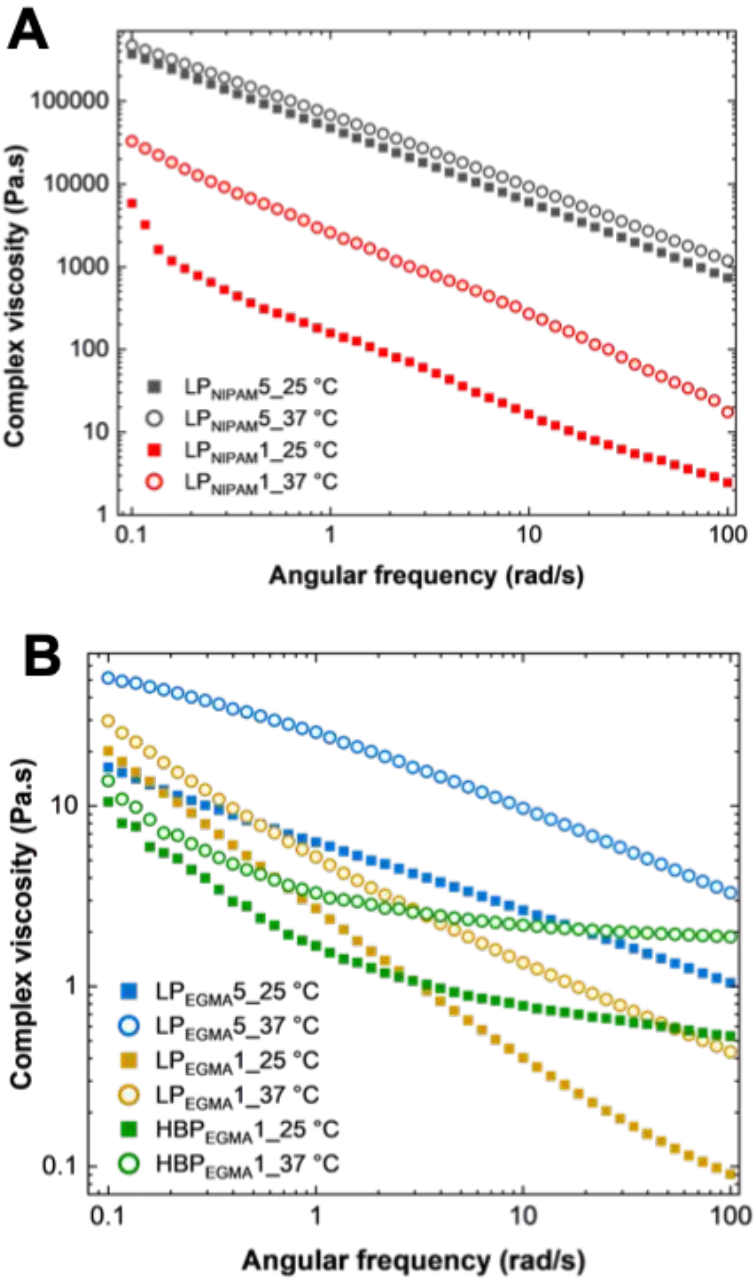

Figure 8. Complex viscosity (η*) as a function of angular frequency (ω) for NIPAM-based TFPs at 15 wt% (left) and EGMA-based TFPs at 30 wt% (right) in PBS, measured at 25°C and 37°C.

3. Conclusion

We developed and systematically investigated TFPs based on two thermoresponsive families (PNIPAM and PEGMA) bearing covalently incorporated fluorescein, and examined how composition, fluorophore loading, and architecture (linear vs. hyperbranched) govern fluorescence across thermally induced phase transitions. The emerging structure–property picture can be summarized as a set of design rules: (i) fluorophore loading sets the sign of the thermoresponse—

View Article Online
DOI: 10.1039/D6PY00425C

low loading (~1 mol%) gives collapse-driven enhancement near T_{cp} followed by quenching, whereas high loading (~5 mol%) gives predominantly quenching, independent of backbone family; (ii) the net hydrophilic–hydrophobic balance (OEGMA/DEGMA ratio, TEGMA and FluA content) and architecture tune T_{cp}, with hyperbranching shifting it upward via chain-end hydration; (iii) aggregation above a threshold concentration is required for a pronounced response; (iv) the response is maximal near neutral pH, where the dye is emissive and partly ionized; and (v) crossing the T_{cp} increases complex viscosity, with hyperbranched topology producing a distinct, weakly-entangled flow signature. Together these rules indicate that thermoresponsive fluorescence is not governed by any single parameter but emerges from the combined effects of composition, fluorophore distribution, and architecture.

We note an important limitation that also frames how these rules should be used. Because synthetic and solubility constraints prevented changing every variable in strict isolation, several parameters co-vary across the sample set (for example, composition, loading, and architecture differ simultaneously between certain pairs), so individual phenomena cannot always be cleanly decoupled. The rules above are therefore best read as directional guidelines extracted within controlled compositional windows rather than as fully orthogonal, quantitative laws. A targeted follow-up series—matching molecular weight and per-chain fluorophore count while varying a single structural variable at a time, and reporting per-fluorophore-normalized intensities—would allow these relationships to be isolated quantitatively. With that caveat, this work provides a practical foundation for rationally tuning fluorescence responses in thermoresponsive polymers toward adaptable optical sensing platforms.

Author contributions

K. Raheja: Data curation, formal analysis, investigation, methodology, validation, visualization, writing–original draft, writing–review & editing; S. Beilharz: Data curation, formal analysis, methodology, validation, visualization, writing–original draft, writing–review & editing; A. Lalam: Data curation, validation, writing–review & editing; Md B. Hasan: Data curation, formal analysis, methodology, writing–review & editing; D. Mathur: Methodology, supervision, resources, writing–review & editing; M. Karayilan: Conceptualization, methodology, project administration, resources, supervision, writing–original draft, writing–review & editing.

Data availability

The data supporting this article have been included as part of the ESI.

Conflict of interest

The authors have no competing financial interests.

Acknowledgements

View Article Online
DOI: 10.1039/D6PY00425C

This work was supported by funding from Case Western Reserve University and the donors of ACS Petroleum Research Fund with a Doctoral New Investigator (DNI) award (PRF# 68078-DNI7).

References.

1. M. A. C. Stuart, W. T. S. Huck, J. Genzer, M. Müller, C. Ober, M. Stamm, G. B. Sukhorukov, I. Szleifer, V. V. Tsukruk, M. Urban, F. Winnik, S. Zauscher, I. Luzinov and S. Minko, Nature Materials, 2010, 9, 101–113.
2. D. Roy, J. N. Cambre and B. S. Sumerlin, Progress in Polymer Science, 2010, 35, 278–301.
3. J. F. Mano, Advanced Engineering Materials, 2008, 10, 515–527.
4. M. Wei, Y. Gao, X. Li and M. J. Serpe, Polymer Chemistry, 2017, 8, 127–143.
5. F. Liu and M. W. Urban, Progress in Polymer Science, 2010, 35, 3–23.
6. C. d. l. H. Alarcón, S. Pennadam and C. Alexander, Chemical Society Reviews, 2005, 34, 276–285.
7. M. S. Shim and Y. J. Kwon, Advanced Drug Delivery Reviews, 2012, 64, 1046–1059.
8. S. S. Das, P. Bharadwaj, M. Bilal, M. Barani, A. Rahdar, P. Taboada, S. Bungau and G. Z. Kyzas, Polymers, 2020, 12, 1397.
9. Q. Zhang, C. Weber, U. S. Schubert and R. Hoogenboom, Materials Horizons, 2017, 4, 109–116.
10. J.-F. Lutz, Ö. Akdemir and A. Hoth, Journal of the American Chemical Society, 2006, 128, 13046–13047.
11. H. Ercan, S. Durkut, A. Koc-Demir, A. E. Elçin and Y. M. Elçin, in *Novel Biomaterials for Regenerative Medicine*, eds. H. J. Chun, K. Park, C.-H. Kim and G. Khang, Springer Nature Singapore, Singapore, 2018, https://doi.org/10.1007/978-981-13-0947-2_10, pp. 163–182.
12. V. Pertici, C. Pin-Barre, C. Rivera, C. Pellegrino, J. Laurin, D. Gigmes and T. Trimaille, Biomacromolecules, 2019, 20, 149–163.
13. X. Song, Z. Zhang, J. Zhu, Y. Wen, F. Zhao, L. Lei, N. Phan-Thien, B. C. Khoo and J. Li, Biomacromolecules, 2020, 21, 1516–1527.
14. S. Geng, H. Zhao, G. Zhan, Y. Zhao and X. Yang, ACS Applied Materials & Interfaces, 2020, 12, 7995–8005.
15. J. Wu, Q. Chen, C. Deng, B. Xu, Z. Zhang, Y. Yang and T. Lu, Theranostics, 2020, 10, 9843–9864.
16. A. K. Singh Chandel, D. Kannan, B. Nutan, S. Singh and S. K. Jewrajka, Journal of Materials Chemistry B, 2017, 5, 4955–4965.
17. S. Beilharz, M. K. Debnath, D. Vinella, A. J. Shoffstall and M. Karayilan, ACS Applied Bio Materials, 2024, 7, 8076–8101.
18. M. Heskins and J. E. Guillet, Journal of Macromolecular Science: Part A - Chemistry, 1968, 2, 1441–1455.
19. H. G. Schild, Progress in Polymer Science, 1992, 17, 163–249.
20. E. J. Kim and D. O. Shah, Langmuir, 2002, 18, 10105–10108.
21. Y. Yuan, K. Raheja, N. B. Milbrandt, S. Beilharz, S. Tene, S. Oshabaheebwa, U. A. Gurkan, A. C. S. Samia and M. Karayilan, RSC Applied Polymers, 2023, 1, 158–189.

View Article Online
DOI: 10.1039/D6PY00425C

22. Y. Zhang, S. Furyk, D. E. Bergbreiter and P. S. Cremer, Journal of the American Chemical Society, 2005, 127, 14505–14510.
23. C. Porsch, S. Hansson, N. Nordgren and E. Malmström, Polymer Chemistry, 2011, 2, 1114–1123.
24. J. Liu, L. Jiang, S. He, J. Zhang and W. Shao, Chemical Engineering Journal, 2022, 433, 133496.
25. J.-F. Lutz, Journal of Polymer Science Part A: Polymer Chemistry, 2008, 46, 3459–3470.
26. R. B. Greenwald, Y. H. Choe, J. McGuire and C. D. Conover, Advanced Drug Delivery Reviews, 2003, 55, 217–250.
27. M. Behzad Khoshgoee, M. Kumar Debnath, G. Pardo, Y. Yuan, M. Zeeshan, E. Mao, T. G. Gray, B. Gurkan, M. J. Bertin and M. Karayilan, RSC Applied Polymers, 2026, https://doi.org/10.1039/D5LP00379B.
28. C. R. Becer, S. Hahn, M. W. M. Fijten, H. M. L. Thijs, R. Hoogenboom and U. S. Schubert, Journal of Polymer Science Part A: Polymer Chemistry, 2008, 46, 7138–7147.
29. J.-F. Lutz, J. Andrieu, S. Üzgün, C. Rudolph and S. Agarwal, Macromolecules, 2007, 40, 8540–8543.
30. S. Uchiyama, Y. Matsumura, A. P. de Silva and K. Iwai, Analytical Chemistry, 2003, 75, 5926–5935.
31. X. Feng, F. Lv, L. Liu, H. Tang, C. Xing, Q. Yang and S. Wang, ACS Applied Materials & Interfaces, 2010, 2, 2429–2435.
32. Y. Yuan, S. Beilharz, H. R. Everson, N. Nupnar, M. K. Debnath, D. Vinella, J. M. Urueña, F. H. Örge, M. J. A. Hore, D. Mathur and M. Karayilan, Biomacromolecules, 2025, 26, 1234–1250.
33. W. Shi, S. He, M. Wei, D. G. Evans and X. Duan, Advanced Functional Materials, 2010, 20, 3856–3863.
34. L. Tang, J. K. Jin, A. Qin, W. Zhang Yuan, Y. Mao, J. Mei, J. Zhi Sun and B. Zhong Tang, Chemical Communications, 2009, https://doi.org/10.1039/B907382E4974–4976.
35. C. Ma, T. Han, N. Niu, L. Al-Shok, S. Efstathiou, D. Lester, S. Huband and D. Haddleton, Polymer Chemistry, 2022, 13, 58–68.
36. Y. Zheng, G. Li, H. Deng, Y. Su, J. Liu and X. Zhu, Polymer Chemistry, 2014, 5, 2521–2529.
37. Y.-J. Jin, R. Dogra, I. W. Cheong and G. Kwak, ACS Applied Materials & Interfaces, 2015, 7, 14485–14492.
38. K. Okabe, N. Inada, C. Gota, Y. Harada, T. Funatsu and S. Uchiyama, Nature Communications, 2012, 3, 705.
39. G. Gao, D. Busko, S. Kauffmann-Weiss, A. Turshatov, I. A. Howard and B. S. Richards, Journal of Materials Chemistry C, 2018, 6, 4163–4170.
40. G. Feng, H. Zhang, X. Zhu, J. Zhang and J. Fang, Biomaterials Science, 2022, 10, 1855–1882.
41. T. Barilero, T. Le Saux, C. Gosse and L. Jullien, Analytical Chemistry, 2009, 81, 7988–8000.
42. D. Wang, R. Miyamoto, Y. Shiraishi and T. Hirai, Langmuir, 2009, 25, 13176–13182.
43. K. Iwai, Y. Matsumura, S. Uchiyama and A. P. de Silva, Journal of Materials Chemistry, 2005, 15, 2796–2800.
44. M. Justo-Tirado, J. Escorihuela, E. Zaballos-García, G. Mínguez Espallargas and J. Pérez-Prieto, Chemistry – A European Journal, 2026, n/a, e03276.

View Article Online
DOI: 10.1039/D6PY00425C

45. H. Kobayashi, M. Nishikawa, C. Sakamoto, T. Nishio, H. Kanazawa and T. Okano, Analytical Sciences, 2009, 25, 1043–1047.
46. J. Hu, X. Zhang, D. Wang, X. Hu, T. Liu, G. Zhang and S. Liu, Journal of Materials Chemistry, 2011, 21, 19030–19038.
47. Y. Shu, R. Song, A. Zheng, J. Huang, M. Chen and J. Wang, Talanta, 2018, 181, 278–285.
48. A. Yamada, Y. Hiruta, J. Wang, E. Ayano and H. Kanazawa, Biomacromolecules, 2015, 16, 2356–2362.
49. G. Liang, J. Wu, H. Gao, Q. Wu, J. Lu, F. Zhu and B. Z. Tang, ACS Macro Letters, 2016, 5, 909–914.
50. A. Seeboth, D. Lötzsch, R. Ruhmann and O. Muehling, Chemical Reviews, 2014, 114, 3037–3068.
51. E. Lee, B. Hammer, J.-K. Kim, Z. Page, T. Emrick and R. C. Hayward, Journal of the American Chemical Society, 2011, 133, 10390–10393.
52. A. Hori, A. Matsumoto, J. Ikenouchi and G.-i. Konishi, Journal of the American Chemical Society, 2025, 147, 9953–9961.
53. J. Luo, Z. Xie, J. W. Y. Lam, L. Cheng, H. Chen, C. Qiu, H. S. Kwok, X. Zhan, Y. Liu, D. Zhu and B. Z. Tang, Chemical Communications, 2001, https://doi.org/10.1039/B105159H1740–1741.
54. Y. Hong, J. W. Y. Lam and B. Z. Tang, Chemical Society Reviews, 2011, 40, 5361–5388.
55. J. Guan, C. Shen, J. Peng and J. Zheng, The Journal of Physical Chemistry Letters, 2021, 12, 4218–4226.
56. W. Z. Yuan, P. Lu, S. Chen, J. W. Y. Lam, Z. Wang, Y. Liu, H. S. Kwok, Y. Ma and B. Z. Tang, Advanced Materials, 2010, 22, 2159–2163.
57. A. Nagai, K. Kokado, J. Miyake and Y. Cyujo, Journal of Polymer Science Part A: Polymer Chemistry, 2010, 48, 627–634.
58. N. Jiang, D. Zhu, Z. Su and M. R. Bryce, Materials Chemistry Frontiers, 2021, 5, 60–75.
59. N. Uehara, Y. Masubuchi and A. Inagawa, Colloids and Surfaces A: Physicochemical and Engineering Aspects, 2021, 618, 126459.
60. C. Gao, M. K. Hossain, M. A. Wahab, J. Xiong, B.-M. Qiu, H. Luo and W. Li, Dyes and Pigments, 2019, 160, 909–914.
61. K. Raheja, A. Shorin, D. G. Gagnon, R. Lutz, M. B. Hasan, M. Singh, S. M. Parker, S. Morozova and M. Karayilan, Journal of Polymer Science, 2025, 63, 5115–5130.
62. C. J. Hawker, R. Lee and J. M. J. Frechet, Journal of the American Chemical Society, 1991, 113, 4583–4588.
63. M. Luzon, C. Boyer, C. Peinado, T. Corrales, M. Whittaker, L. Tao and T. P. Davis, Journal of Polymer Science Part A: Polymer Chemistry, 2010, 48, 2783–2792.
64. Y. H. Kim and O. W. Webster, Journal of the American Chemical Society, 1990, 112, 4592–4593.
65. H. Chen and J. Kong, Polymer Chemistry, 2016, 7, 3643–3663.
66. Z. Fang, S. Sun, Y. Gu, X. Li, C. Yang, F. Liu, X. Lin and Z. Wang, Advanced Functional Materials, 2026, n/a, e75590.
67. F. Román, P. Colomer, Y. Calventus and J. M. Hutchinson, Materials, 2016, 9, 192.
68. D. Wang and T. Imae, Journal of the American Chemical Society, 2004, 126, 13204–13205.
69. P. Wang, X. Wang, K. Meng, S. Hong, X. Liu, H. Cheng and C. C. Han, Journal of Polymer Science Part A: Polymer Chemistry, 2008, 46, 3424–3428.

View Article Online
DOI: 10.1039/D6PY00425C

70. C. M. Nunez, B.-S. Chiou, A. L. Andrady and S. A. Khan, Macromolecules, 2000, 33, 1720–1726.
71. S. Habibu, N. M. Sarih, N. A. Sairi and M. Zulkifli, Royal Society Open Science, 2019, 6.
72. B. I. Voit and A. Lederer, Chemical Reviews, 2009, 109, 5924–5973.
73. C. Cunha, P. Klein, C. Rosenauer, U. Scherf and J. S. Seixas de Melo, Macromolecules, 2021, 54, 7612–7620.
74. S.-H. Kim, I.-J. Hwang, S.-Y. Gwon and Y.-A. Son, Dyes and Pigments, 2010, 87, 84–88.
75. Q. Shen, C. Fang, L. Hu and M. J. Serpe, SmartMat, 2024, 5, e1254.
76. M. Oh, Y. Yoon and T. S. Lee, RSC Advances, 2020, 10, 39277–39283.
77. D. Wang, T. Liu, J. Yin and S. Liu, Macromolecules, 2011, 44, 2282–2290.
78. C. K. Chee, S. Rimmer, D. A. Shaw, I. Soutar and L. Swanson, Macromolecules, 2001, 34, 7544–7549.
79. A. J. Convertine, N. Ayres, C. W. Scales, A. B. Lowe and C. L. McCormick, Biomacromolecules, 2004, 5, 1177–1180.
80. A. P. Vogt and B. S. Sumerlin, Macromolecules, 2008, 41, 7368–7373.
81. G. Moad, E. Rizzardo and S. H. Thang, Chemistry – An Asian Journal, 2013, 8, 1634–1644.
82. D. Roy, W. L. A. Brooks and B. S. Sumerlin, Chemical Society Reviews, 2013, 42, 7214–7243.
83. J.-F. Lutz and A. Hoth, Macromolecules, 2006, 39, 893–896.
84. J. Heyda, S. Soll, J. Yuan and J. Dzubiella, Macromolecules, 2014, 47, 2096–2102.
85. Q. Duan, A. Narumi, Y. Miura, X. Shen, S.-I. Sato, T. Satoh and T. Kakuchi, Polymer Journal, 2006, 38, 306–310.
86. T. Despres, T. Fabre, S. Legeay, G. Bastiat, F. D'Agosto, M. Lansalot, M. S. M. Pearson-Long, S. Piogé and S. Pascual, Macromolecules, 2024, 57, 2421–2431.
87. U. Haldar, S. G. Roy and P. De, Polymer, 2016, 97, 113–121.
88. S. Ghosh Roy and P. De, Polymer Chemistry, 2014, 5, 6365–6378.
89. B. McLeland, D. Afsar, A. I. Mudiyanselage and P. R. Calvo, Polymer, 2026, 347, 129699.
90. S. Bener, C. Aydogan and Y. Yagci, Macromolecular Chemistry and Physics, 2021, 222, 2000408.
91. J. A. Alfurhood, H. Sun, P. R. Bachler and B. S. Sumerlin, Polymer Chemistry, 2016, 7, 2099–2104.
92. M. K. Debnath, N. Nupnar, Y. Yuan, E. R. Kone, V. O. Rodionov, M. J. A. Hore and M. Karayilan, Macromolecules, 2025, 58, 9930–9943.
93. Ł. Otulakowski, M. Kasprów, A. Strzelecka, A. Dworak and B. Trzebicka, Polymers, 2021, 13, 90.
94. M. Matsuura, M. Ohshima, Y. Hiruta, T. Nishimura, K. Nagase and H. Kanazawa, International Journal of Molecular Sciences, 2018, 19, 1646.
95. F. Le Guern, V. Mussard, A. Gaucher, M. Rottman and D. Prim, International Journal of Molecular Sciences, 2020, 21, 9217.
96. S. P. Prieto, K. K. Lai, J. A. Laryea, J. S. Mizell, W. C. Mustain and T. J. Muldoon, Biomed. Opt. Express, 2017, 8, 2324–2338.
97. R. Kanno, M. Ouchi and T. Terashima, Polymer Chemistry, 2023, 14, 1718–1726.
98. R. Freitag and F. Garret-Flaudy, Langmuir, 2002, 18, 3434–3440.
99. J. Woo, H. Park, Y. Na, S. Kim, W. I. Choi, J. H. Lee, H. Seo and D. Sung, RSC Advances, 2020, 10, 2998–3004.

View Article Online
DOI: 10.1039/D6PY00425C

100. M. M. Martin and L. Lindqvist, Journal of Luminescence, 1975, 10, 381–390.
101. M. V. Quental, H. Passos, K. A. Kurnia, J. A. P. Coutinho and M. G. Freire, Journal of Chemical & Engineering Data, 2015, 60, 1674–1682.
102. Y. Kim, D. Kim, G. Jang, J. Kim and T. S. Lee, Sensors and Actuators B: Chemical, 2015, 207, 623–630.

View Article Online
DOI: 10.1039/D6PY00425C

Data Availability Statement

Thermoresponsive Fluorescent Polymers: Influence of Size, Composition, and Architecture

Konpal Raheja,[a] Sophia Beilharz,[a] Ajitesh Lalam,[a] Md. Bablu Hasan,[a] Divita Mathur,[a] Metin Karayilan[a,] *

[a] Department of Chemistry, Case Western Reserve University. Cleveland, OH 44106 USA

The data supporting this article have been included as part of the ESI.